Step-guided epitaxial growth of blue phosphorene on vicinal Ag(111)

Chao He,[1] Shaogang Xu,[1] Xingxing Dong,[1] Changchun He,[1] Xiangting Hu,[1] Guang Liu,[1] and Hu Xu[1,2,*]
[1]*Department of Physics, Southern University of Science and Technology, Shenzhen 518055, People's Republic of China*
[2]*Quantum Science Center of Guangdong-Hong Kong-Macao Greater Bay Area (Guangdong), Shenzhen 518045, People's Republic of China*

(Received 30 September 2022; revised 4 February 2023; accepted 17 March 2023; published 27 March 2023)

Blue phosphorene (blue-P) is a promising candidate for developing next-generation nanoelectronics devices due to its unique properties. Therefore, the controllable growth of a two-dimensional (2D) wafer-scale blue-P monolayer on substrates is a fundamental issue. However, the direct growth of blue-P on substrates currently remains a daunting challenge. In this paper, by using first-principles calculations, we propose a feasible route for fabricating blue-P via epitaxial growth. The growth mechanism of one-dimensional (1D) phosphorene chains to finite-sized blue-P clusters on Ag(111) is elucidated, and the reason why blue-P clusters cannot grow into a large-area monolayer on the Ag(111) surface is revealed. Moreover, the growth of blue-P on vicinal Ag(111) is explored and the energetic benefit of 1D zigzag blue-P nanoribbon growth along the Ag⟨110⟩ step edge is confirmed. More importantly, we propose that the unidirectionally orientated blue-P nanoribbons can merge into large-area blue-P nanosheets through a step-guide growth mode. The feasibility of this strategy is validated by using molecular dynamics simulations, and a series of candidate substrates is selected. This study not only provides a promising substrate for epitaxial growth of blue-P but also sheds light on the preparation of more 2D materials.

DOI: 10.1103/PhysRevMaterials.7.034003

I. INTRODUCTION

As graphene [1] analogs, monoelemental two-dimensional (2D) materials have attracted great interest for their potential applications [2–7]. Among them, blue phosphorene (blue-P [3]) has received much attention due to its promising properties [8–10]. However, unlike black phosphorene (black-P) [4], which can be mechanically exfoliated from its layered bulk crystal, blue-P can only be fabricated by bottom-up epitaxy due to the lack of a corresponding bulk counterpart. Although the experimental synthesis of 2D blue-P on Au(111) was first reported in 2016 [11], it has been confirmed recently to be the Au-P network [12,13] rather than blue-P on Au(111). Subsequently, we further reported that metal phosphides are formed on more chemically active Cu(111) [14] and Pt(111) [15]. To date, extensive efforts have been made both theoretically and experimentally for the epitaxial growth of blue-P [11,14,16–22]. Of particular notice, recent experiments proposed that blue-P was realized by preparing Au-Si [19] and Cu_3O_2 [20] buffer layers on Au(111) and Cu(111), respectively, but it is still challenging to uncover the underlying growth mechanism of blue-P on such extremely complicated substrates.

Unlike the metal substrates mentioned above, the deposition of P atoms on the Ag(111) surface yields monoelemental phosphorus materials [23,24], which is similar to the case that silicene can only be prepared on Ag(111) [25–27]. However, even under different experimental conditions, only one-dimensional (1D) phosphorene chains [23] and blue-P clusters [24] were obtained on the Ag(111) surface, and the desired blue-P monolayer is still not prepared. Although the presence of these blue-P chains and clusters has been attributed to non-negligible vertical interlayer interactions between P and Ag(111) [14,23,24], a systematic study on their growth mechanisms is still lacking. Nevertheless, the crystalline 1D P chains still provide a platform for the verification of predicted properties [28–31] and for the continued preparation of phosphorene nanoribbons [23]. For discrete blue-P clusters obtained on the Ag(111) surface at higher P coverage [24], the realization of their patching might enable the fabrication of large-area blue-P nanosheets. Notably, several theoretical works have proposed the utilization of steps to induce the unidirectional growth of 2D materials [32–34]. Recently, large-area graphene [35,36], hexagonal boron nitride (h-BN) [37,38], and transition metal dichalcogenides [39–42] have been experimentally prepared using high-index surfaces. Compared to these 2D materials, which have their corresponding layered compounds, blue-P has relatively weak intralayer interactions [14,43,44] and screening for a suitable stepped surface may require additional requirements. However, the intrinsic roles played by steps on the unidirectional nucleation and epitaxial growth of blue-P are lacking. Therefore, it is promising to investigate the controlled preparation of blue-P on vicinal Ag(111).

In this paper, based on extensive density functional theory (DFT) calculations, we present a feasible route for synthesizing a blue-P monolayer via epitaxial growth. First, through thermodynamic phase diagrams, we explain the experimentally observed structures of 1D phosphorene chains and blue-P clusters, confirming that blue-P clusters are more energetically favorable on Ag(111). Subsequently, parallel to borophene 1D nucleation on step edges [34], we here explore

*xuh@sustech.edu.cn

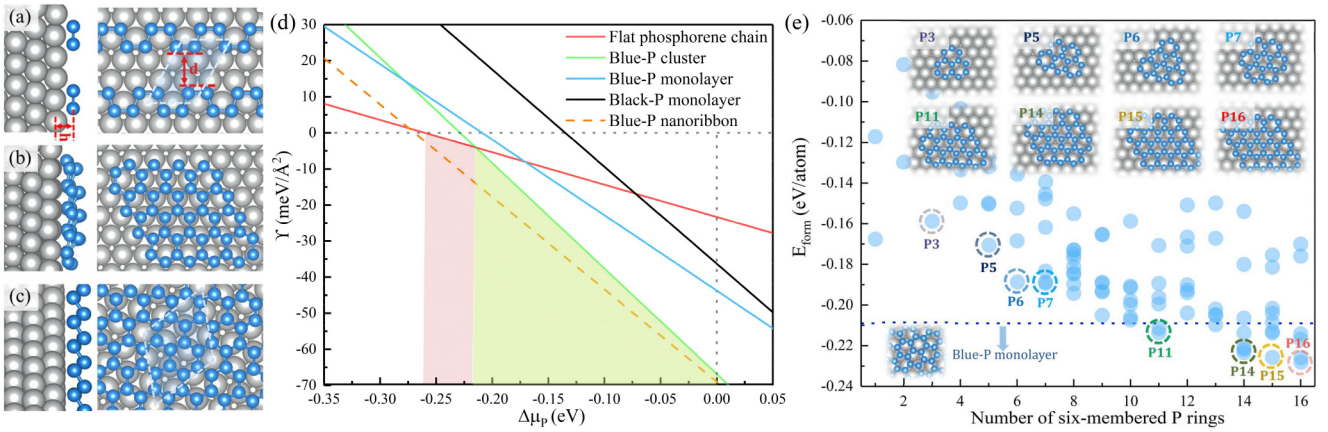

FIG. 1. Top and side views of atomic structures of (a) a phosphorene chain array on the (2 × 3) Ag(111) supercell, (b) a blue-P cluster on the (7 × 7) Ag(111) supercell, and (c) a ($\sqrt{7} \times \sqrt{7}$) blue-P monolayer on the (3 × 3) Ag(111) supercell. (d) Phase diagram of various phosphene structures. (e) Formation energy as a function of the number of six-membered P rings. The atomic structures of P clusters highlighted by dashed circles are provided. Gray and blue spheres represent Ag and P atoms, respectively.

the growth of blue-P on vicinal Ag(111) and confirm the energetic benefits of 1D blue-P nanoribbon growth along the ⟨110⟩ step edge. Furthermore, by *ab initio* molecular dynamics (AIMD) simulations, we propose a step-guide growth mode of blue-P on the Ag(223) surface, and a series of high-index Ag facets are screened out for the epitaxial growth of blue-P. Our work provides valuable insights into the synthesis of blue-P nanoribbons and wafer-scale blue-P thin films.

II. COMPUTATIONAL METHODS

All the *ab initio* calculations are performed by using the Vienna *ab initio* simulation package (VASP) [45,46]. The projector augmented-wave approach (PAW) with the Perdew-Burke-Ernzerhof (PBE) generalized gradient approximation [47] is used for structural optimization and total energy calculations. The semiempirical dispersion-corrected DFT-D3 [48] method is employed to account for the van der Waals (vdW) interaction. The force convergence criteria and kinetic energy cutoff are set at 0.02 eV/Å and 350 eV, respectively. The *k*-point mesh is sampled by a separation of about 0.03/Å, and the thickness of the vacuum layer is 15 Å to avoid an interaction between two neighboring images. The bottom layers of substrates are fixed at their bulk positions and other layers are further relaxed during geometry optimization.

III. RESULTS AND DISCUSSION

The blue-P chain, cluster, and monolayer on the Ag(111) surface are shown in Figs. 1(a)–1(c), respectively. 1D P chains were experimentally observed [23] on the Ag(111) surface at room temperature. At lower concentrations of P atoms, P atoms prefer to self-assemble to form a (2 × 3) superstructure with a distance (d) of 5.51 Å between two adjacent P chains, as shown in Fig. 1(a). Unlike the buckled honeycomb blue-P, the armchair-shaped chains have negligible corrugation and the height (h) of the chains above the Ag(111) surface is about 2.24 Å. Considering that the sum of the covalent radii of the P (1.11 Å) and Ag (1.28 Å) atoms is 2.39 Å, this distance indicates the existence of a strong chemical bonding between P and Ag(111). In addition, cluster-structural blue-P grown on the Ag(111) surface at a substrate temperature of 420 K was also reported recently [24], and the proposed 4 × 4 nanoflake of blue-P is shown in Fig. 1(b). Compared to the extended blue-P monolayer in Fig. 1(c), the P atoms at the edges of blue-P clusters are strongly bonded with the surface Ag atoms, leading to some degree of distortion at the cluster edges, which is in excellent agreement with the experimental observation that the inner blue-P islands are brighter than those at the edges [24]. The formation energies (E_{form}) of a 1D P chain array, blue-P cluster, and blue-P monolayer are −0.260, −0.229, and −0.209 eV/atom, respectively (see the Supplemental Material for details [49]), indicating that the experimentally observed chains and clusters are indeed more energetically favorable than the blue-P monolayer.

The formation energy per area for the heterogeneous structure relative to the clean substrate is denoted as γ [49]. As shown in Fig. 1(d), the P chemical potential in its bulk black phosphorus is marked by the vertical dotted line and the clean surface ($\gamma = 0$) is indicated by the horizontal dotted line. Higher $\Delta\mu_{\text{P}}$ corresponds to higher P coverages. For the P chain superstructure on the 2 × 3 Ag(111) substrate, four P atoms deposited on the surface of the 2 × 3 supercell, corresponding to a P coverage of 0.67. It is worth noting that the ordered P chain array is more stable than the clean surface when $-0.265 \leqslant \Delta\mu_{\text{P}} < -0.215$ eV. Moreover, we further consider an individual P chain on the Ag(111) surface [49], which is indeed more energetically superior at lower coverage compared to blue-P clusters [50]. When $\Delta\mu_{\text{P}}$ is in the range of −0.215 to 0 eV, the blue-P clusters are more stable compared to the blue-P monolayer, which is consistent with the fact that blue-P clusters were still obtained experimentally at a P atom coverage above 0.8 [50]. This suggests that the energetically preferred one is not the blue-P monolayer even when the P coverage is further increased. In addition, we calculate γ of the black-P monolayer, and we find that the black-P monolayer is also energetically unfavorable on Ag(111). These results are in good agreement with both experimental and theoretical reports [18,23,24,50,51].

To further explain the growth behavior of the blue-P monolayer on the Ag(111) surface, we consider more blue-P clusters on Ag(111) to check the evolution of E_{form}. It is worth noting that these blue-P clusters consisting of hexagons do not represent a sequential process of initial nucleation, and the transition from 1D chains to 2D clusters can be found by considering the atom-by-atom growth sequence [49]. With the expansion of the blue-P cluster size, as shown in Fig. 1(e), E_{form} decreases first due to the self-assembly behavior of blue-P clusters. However, when the number of six-membered P_6 rings reaches 11, E_{form} starts to be lower than that of the blue-P monolayer. Notably, when the edge length reaches four P_6 rings, E_{form} is lower than that of the blue-P monolayer. For clusters with edge lengths greater than four P_6 rings, E_{form} turns to increase (see Fig. S1 [49]), which certainly limits the size of blue-P clusters. Indeed, the experimentally observed clusters with edge lengths larger than six P_6 rings rarely occur [24]. In addition, when we compare clusters with the same number of P_6 rings, clusters with trapezoidal and hexagonal shapes [see the insets in Fig. 1(e)] have lower E_{form} highlighted by the dashed circles, which is also in good agreement with the experimental observations [24]. Based on the above results, we explain the experimental phenomena reported so far from the theoretical viewpoint. This surface-limited growth mode can be attributed to the strong interaction between P and Ag(111) [14,24], while the regularly arranged blue-P clusters facilitate the release of compressive strain. An alternative strategy by breaking the surface-limited growth mode to prepare a large-area blue-P monolayer is highly desired.

Steps are inevitable on metal surfaces, and it has been demonstrated experimentally that blue-P clusters appear at the steps on the Ag(111) surface [24], but their edge structures are not clear. An ultrahigh-vacuum experimental condition or annealing help avoid the possible passivation of oxygen atoms at step edges. As shown in Fig. S2 [49], we consider the armchair-shaped and zigzag-shaped chains growing on the vicinal Ag(111) and flat Ag(111) surfaces, respectively. We further define $\Delta E_{\text{form}} = E_{\text{form}}^{\text{ac}} - E_{\text{form}}^{\text{zz}}$ to describe the interaction difference between the formation energies of armchair-shaped chains ($E_{\text{form}}^{\text{ac}}$) and zigzag-shaped chains ($E_{\text{form}}^{\text{zz}}$) adsorbed on substrates. On the flat Ag(111) surface, ΔE_{form} is -0.082 eV/atom, which explains the armchair-shaped structure that appears experimentally on the terrace. In contrast, ΔE_{form} becomes 0.040 eV/atom when two phosphorene chains are grown on the vicinal Ag(111) surface, which makes the zigzag-shaped chains with more contact with the step more promising to grow along the Ag⟨110⟩ step.

We next consider the case at a higher P coverage on the vicinal Ag(111). In Figs. 2(a) and 2(b), we respectively show the blue-P nanoribbons with armchair and zigzag edges along the Ag⟨110⟩ step, and the corresponding E_{form} are -0.239 and -0.269 eV/atom, indicating that blue-P nanoribbons with zigzag edges are more favorable. To determine the decisive factor in the unidirectional growth of blue-P with zigzag edges, we compare the contact energies [32] of blue-P nanoribbons with zigzag edges, which are 1.700 and 1.562 eV/Å for the step and surface growth modes, respectively. The energy difference of 0.138 eV/Å suggests that the step has a

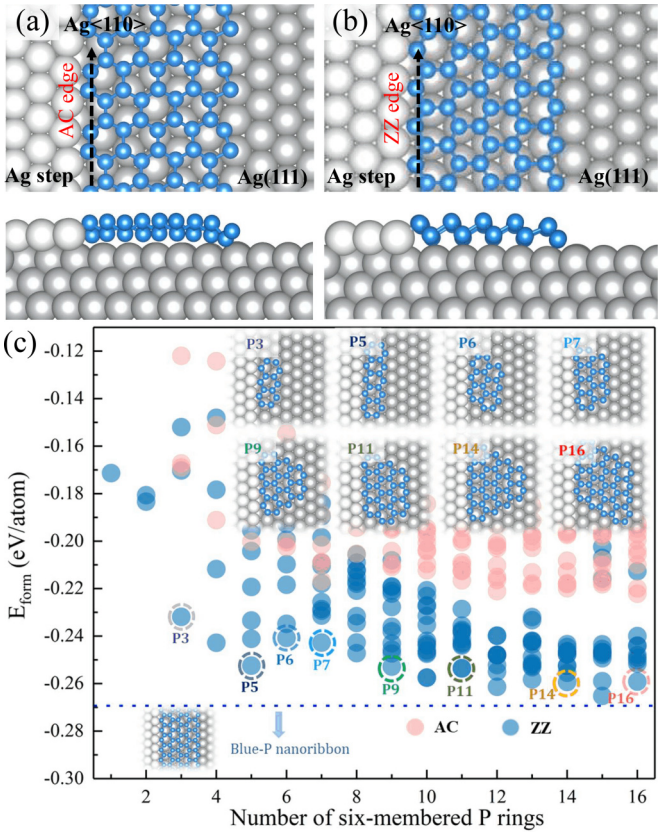

FIG. 2. Top and side views of (a) armchair and (b) zigzag nanoribbons on the vicinal Ag(111) surface. White spheres represent stepped Ag atoms. (c) Formation energy as a function of the number of six-membered P rings along the Ag⟨110⟩ step. The atomic structures of P clusters highlighted by dashed circles are provided. The dark blue and pink circles represent clusters of blue-P with zigzag edges and armchair edges, respectively.

significant modulating effect on zigzag-shaped nanoribbons, which ultimately leads to the step-guided growth of blue-P nanoribbons. In addition, as shown by the dashed line in Fig. 1(d), the zigzag-shaped nanoribbons that grow along the Ag⟨110⟩ step have the lowest γ in comparison with other phosphene structures, showing the possibility of experimental preparation.

To further explore the growth process of blue-P along the step, we consider the evolution of E_{form} of blue-P clusters along the step. We systematically discuss the case of clusters with an edge length of less than five six-membered P rings. For clusters with longer edges, as shown in Fig. S3 [49], E_{form} of ring-based 1D P_6 chains significantly decrease and gradually converge. As shown in Fig. 2(c), E_{form} decreases as the clusters grow, but the zigzag-shaped clusters in contact with the steps are clearly more superior than the armchair-shaped clusters. Apparently, the length-limited blue-P clusters are first grown along the step and then shift to grow laterally perpendicular to the step. In addition, most of the P clusters grown along the steps are tetragonal and trapezoidal [see the insets in Fig. 2(c)], which can be attributed to the reduced surface symmetry, similar to the experimental growth of MoS_2 at the steps [39]. Unlike the discrete blue-P clusters

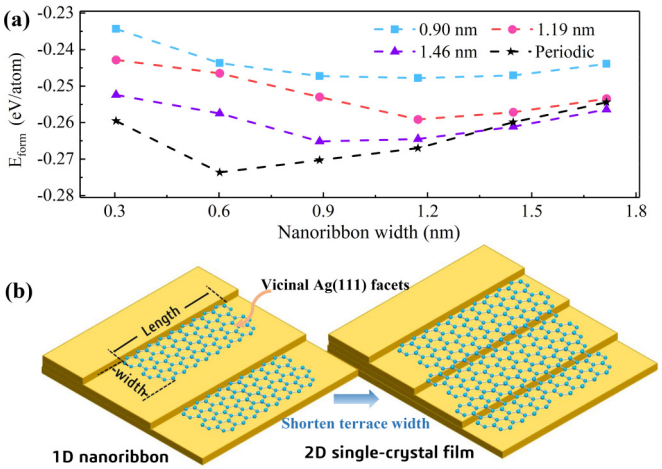

FIG. 3. (a) Formation energy evolution of blue-P clusters and nanoribbons with zigzag edges growing horizontally perpendicular to the Ag⟨110⟩ step. (b) Schematic diagram regarding the growth of blue-P monolayer by merging blue-P nanoribbons.

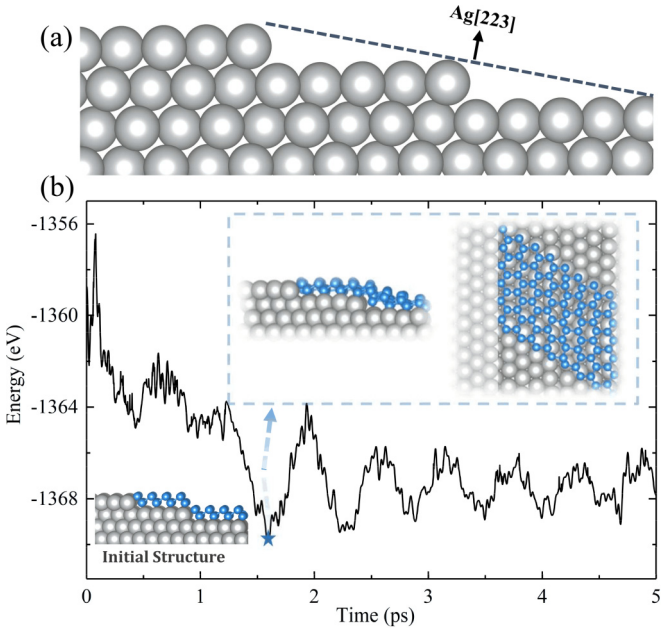

FIG. 4. (a) Side view of Ag(223). (b) Blue-P clusters on Ag(223) after 5-ps AIMD simulations at 300 K.

on the Ag(111) surface, we find that blue-P nanoribbons with a width of four columns of P_6 rings are more energetically favorable, which provides an idea for the growth of blue-P nanoribbons. For the initial nucleation of a blue-P nanoribbon growing along the step, we discuss this in detail in the Supplemental Material [49]. The preference of P atoms for 1D nucleation at the step edge is confirmed, which is similar to the 1D growth behavior of borophene at the h-BN step edge [34].

To quantitatively evaluate the role of the Ag step in tuning the growth of blue-P nanoribbons, we calculate E_{form} as a function of the width perpendicular to the step. As shown in Fig. 3(a), E_{form} of clusters with different lengths and nanoribbons exhibit similar decreasing and then increasing characteristics. The length and width of the blue-P nanosheets are illustrated in Fig. 3(b). For finite-sized clusters, E_{form} decreases linearly with a widening of the cluster when its width is less than 0.89 nm, which facilitates the rapid self-assembly of the deposited P atoms along the steps. However, when the width of clusters exceeds 1.17 nm, E_{form} turns to increase linearly, gradually approaching E_{form} of blue-P cluster growth on the Ag(111) surface. Therefore, a unidirectional blue-P cluster will have a critical size, and the surface restriction will still occur at the zigzag edge away from the step when the width of the cluster reaches the critical size. Compared to finite-sized clusters, the minimum of E_{form} for the periodically matched nanoribbon appears earlier, which can be attributed to the effect of reduced edge ratios and lattice mismatch. By linear fitting [49], we can estimate that the width of the nanoribbons can eventually reach 3.22 nm, which have been theoretically predicted to have a wealth of physical properties [52,53].

More intriguingly, after the preparation of blue-P nanoribbons, it is natural to consider how to merge 1D nanoribbons into a 2D large-scale blue-P monolayer. Unlike the healing behavior of h-BN on vicinal Ni(110) [32], to ensure the epitaxial extension of blue-P nanoribbons on vicinal Ag(111), it requires striding across the step, and therefore blue-P nanoribbons are limited by a critical width. Nevertheless, as shown in Fig. 3(b), if we can prepare vicinal surfaces with terrace widths smaller than the critical size of 3.22 nm, it is possible to achieve a docking of blue-P nanoribbons. Usually, high-index surfaces with higher surface energies are more difficult to prepare compared to the Ag(111) surface. Fortunately, it has been experimentally available to prepare the vicinal Ag(111) surface with a step separation of 1.13 nm in width [54], which offers the feasibility of large-scale blue-P epitaxy on Ag surfaces with high step density.

To verify the patching behavior of blue-P nanoribbons across the step, as shown in Fig. 4(a), we chose a specific Ag(223) facet with a step width of 1 nm. The surface energy of Ag(223) is 0.77 J/m^2 [55], which is only 0.01 J/m^2 higher than that of Ag(111). We perform AIMD simulations at 300 K, which is well below the desorption temperature of P atoms on the Ag(111) substrate [24]. As shown in Fig. 4(b), after 1.6 ps of simulation, the two clusters grown on adjacent terraces merge together, which kinetically indicates the possibility of the growth of blue-P nanosheets by patching. Moreover, the total energy of the patched structure is 1.806 eV lower than that of the initial structure, which also indicates that this patching process can easily occur. For periodically matched nanoribbons, as shown in Fig. S4 [49], two nanoribbons grown along the steps are placed on adjacent terraces with a distance of about 3.32 Å between the two nanoribbons, which is much larger than the bond length for blue-P. It is worth noting that the stitched structure still has an energy benefit of 0.505 eV compared to the separated nanoribbons. Finally, we also screen out other high-index facets with lower surface energies and suitable terrace widths, as shown in Table S1 [49], which provides candidate substrates for the experimental synthesis of the large-scale blue-P monolayer.

IV. CONCLUSIONS

In conclusion, this theoretical work presents a way for synthesizing wafer-level single-crystal blue-P monolayer on vicinal Ag(111) substrates. Using extensive DFT calculations, we explain the experimental observations of the deposition of P atoms on the Ag(111) surface and perform a systematic study of the growth mechanism from 1D phosphene chains to blue-P clusters. Moreover, the step edge of Ag(111) is proposed to induce the unidirectional nucleation, growth, and subsequent emergence of zigzag blue-P nanoribbons into a single-crystalline blue-P monolayer. By considering the step width and surface energy, we identify a series of high-index Ag facets as ideal candidates to epitaxially grow blue-P. This work deepens our understanding of phosphene structures and provides a practical approach for preparing large-scale blue-P.

ACKNOWLEDGMENTS

This work is supported by the National Natural Science Foundation of China (Grant No. 11974160), the Science, Technology, and Innovation Commission of Shenzhen Municipality (Grant No. RCYX20200714114523069), and the Center for Computational Science and Engineering at Southern University of Science and Technology.

[1] K. S. Novoselov, A. K. Geim, S. V. Morozov, D.-e. Jiang, Y. Zhang, S. V. Dubonos, I. V. Grigorieva, and A. A. Firsov, Science **306**, 666 (2004).
[2] D. Zhou, H. Li, N. Si, H. Li, H. Fuchs, and T. Niu, Adv. Funct. Mater. **31**, 2006997 (2021).
[3] Z. Zhu and D. Tománek, Phys. Rev. Lett. **112**, 176802 (2014).
[4] L. Li, Y. Yu, G. J. Ye, Q. Ge, X. Ou, H. Wu, D. Feng, X. H. Chen, and Y. Zhang, Nat. Nanotechnol. **9**, 372 (2014).
[5] J. Zhu, C. He, Y.-H. Zhao, and B. Fu, J. Mater. Chem. C **8**, 2732 (2020).
[6] F. Ersan, D. Keçik, V. Özçelik, Y. Kadioglu, O. Ü. Aktürk, E. Durgun, E. Aktürk, and S. Ciraci, Appl. Phys. Rev. **6**, 021308 (2019).
[7] F. Ersan, E. Aktürk, and S. Ciraci, Phys. Rev. B **94**, 245417 (2016).
[8] C. Sevik and H. Sevinçli, Nanotechnology **27**, 355705 (2016).
[9] L. Zhu, S.-S. Wang, S. Guan, Y. Liu, T. Zhang, G. Chen, and S. A. Yang, Nano Lett. **16**, 6548 (2016).
[10] W. Xu, J. Zhao, and H. Xu, J. Phys. Chem. C **122**, 15792 (2018).
[11] J. L. Zhang, S. Zhao, C. Han, Z. Wang, S. Zhong, S. Sun, R. Guo, X. Zhou, C. D. Gu, K. D. Yuan *et al.*, Nano Lett. **16**, 4903 (2016).
[12] H. Tian, J.-Q. Zhang, W. Ho, J.-P. Xu, B. Xia, Y. Xia, J. Fan, H. Xu, M. Xie, and S. Tong, Matter **2**, 111 (2020).
[13] J.-P. Xu, J.-Q. Zhang, H. Tian, H. Xu, W. Ho, and M. Xie, Phys. Rev. Mater. **1**, 061002(R) (2017).
[14] C. He, S. Xu, C. He, X. Dong, F. Yan, X. Hu, and H. Xu, Phys. Rev. Mater. **6**, 064011 (2022).
[15] J. Zhang, X. Dong, S. Xu, Y. Xia, W. Ho, H. Xu, and M. Xie, 2D Mater. **9**, 045002 (2022).
[16] J. Zeng, P. Cui, and Z. Zhang, Phys. Rev. Lett. **118**, 046101 (2017).
[17] Y. Yin, V. Gladkikh, P. Li, L. Zhang, Q. Yuan, and F. Ding, Chem. Mater. **33**, 9447 (2021).
[18] L. Qiu, J. Dong, and F. Ding, Nanoscale **10**, 2255 (2018).
[19] J. L. Zhang, S. Zhao, S. Sun, H. Ding, J. Hu, Y. Li, Q. Xu, X. Yu, M. Telychko, J. Su *et al.*, ACS Nano **14**, 3687 (2020).
[20] D. Zhou, Q. Meng, N. Si, X. Zhou, S. Zhai, Q. Tang, Q. Ji, M. Zhou, T. Niu, and H. Fuchs, ACS Nano **14**, 2385 (2020).
[21] N. Han, N. Gao, and J. Zhao, J. Phys. Chem. C **121**, 17893 (2017).
[22] S. Zhao and Z. Li, J. Phys. Chem. C **125**, 675 (2021).
[23] W. Zhang, H. Enriquez, Y. Tong, A. J. Mayne, A. Bendounan, A. Smogunov, Y. J. Dappe, A. Kara, G. Dujardin, and H. Oughaddou, Nat. Commun. **12**, 5160 (2021).
[24] S. Yang, Z. Hu, W. Wang, P. Cheng, L. Chen, and K. Wu, Chin. Phys. Lett. **37**, 096803 (2020).
[25] B. Feng, B. Fu, S. Kasamatsu, S. Ito, P. Cheng, C.-C. Liu, Y. Feng, S. Wu, S. K. Mahatha, P. Sheverdyaeva *et al.*, Nat. Commun. **8**, 1007 (2017).
[26] B. Feng, Z. Ding, S. Meng, Y. Yao, X. He, P. Cheng, L. Chen, and K. Wu, Nano Lett. **12**, 3507 (2012).
[27] C.-C. He, S.-G. Xu, S.-B. Qiu, C. He, Y.-J. Zhao, X.-B. Yang, and H. Xu, Nanoscale **14**, 12757 (2022).
[28] J. Xie, J. Zhong, and W. Sheng, Phys. Rev. B **105**, 245416 (2022).
[29] F. Yao, M. Xia, Q. Zhang, Q. Wu, O. Terasaki, J. Gao, and C. Jin, Carbon **189**, 467 (2022).
[30] M. Hart, J. Chen, A. Michaelides, A. Sella, M. S. P. Shaffer, and C. G. Salzmann, Inorg. Chem. **58**, 15216 (2019).
[31] F. Ersan, E. Aktürk, and S. Ciraci, Phys. Chem. Chem. Phys. **21**, 14832 (2019).
[32] K. V. Bets, N. Gupta, and B. I. Yakobson, Nano Lett. **19**, 2027 (2019).
[33] J. Dong, L. Zhang, X. Dai, and F. Ding, Nat. Commun. **11**, 5862 (2020).
[34] Q. Ruan, L. Wang, K. V. Bets, and B. I. Yakobson, ACS Nano **15**, 18347 (2021).
[35] Q. Yuan, B. I. Yakobson, and F. Ding, J. Phys. Chem. Lett. **5**, 3093 (2014).
[36] X. Li, G. Wu, L. Zhang, D. Huang, Y. Li, R. Zhang, M. Li, L. Zhu, J. Guo, T. Huang *et al.*, Nat. Commun. **13**, 1773 (2022).
[37] L. Wang, X. Xu, L. Zhang, R. Qiao, M. Wu, Z. Wang, S. Zhang, J. Liang, Z. Zhang, Z. Zhang *et al.*, Nature (London) **570**, 91 (2019).
[38] T.-A. Chen, C.-P. Chuu, C.-C. Tseng, C.-K. Wen, H.-S. P. Wong, S. Pan, R. Li, T.-A. Chao, W.-C. Chueh, Y. Zhang *et al.*, Nature (London) **579**, 219 (2020).
[39] P. Yang, D. Wang, X. Zhao, W. Quan, Q. Jiang, X. Li, B. Tang, J. Hu, L. Zhu, S. Pan *et al.*, Nat. Commun. **13**, 3238 (2022).
[40] P. Yang, S. Zhang, S. Pan, B. Tang, Y. Liang, X. Zhao, Z. Zhang, J. Shi, Y. Huan, Y. Shi *et al.*, ACS Nano **14**, 5036 (2020).

[41] L. Liu, T. Li, L. Ma, W. Li, S. Gao, W. Sun, R. Dong, X. Zou, D. Fan, L. Shao *et al.*, Nature (London) **605**, 69 (2022).
[42] R. Dong, X. Gong, J. Yang, Y. Sun, L. Ma, and J. Wang, Adv. Mater. **34**, 2201402 (2022).
[43] N. Si and T. Niu, Nano Today **30**, 100805 (2020).
[44] J. Gao, G. Zhang, and Y.-W. Zhang, J. Am. Chem. Soc. **138**, 4763 (2016).
[45] G. Kresse and J. Furthmüller, Phys. Rev. B **54**, 11169 (1996).
[46] G. Kresse and J. Furthmüller, Comput. Mater. Sci. **6**, 15 (1996).
[47] P. E. Blöchl, Phys. Rev. B **50**, 17953 (1994).
[48] S. Grimme, J. Antony, S. Ehrlich, and H. Krieg, J. Chem. Phys. **132**, 154104 (2010).
[49] See Supplemental Material at http://link.aps.org/supplemental/10.1103/PhysRevMaterials.7.034003 for computational details and supplemental tables of candidates.
[50] Y. Wang, C. Hua, S. Sun, J. Gou, S. Duan, A. T. S. Wee, M. Zhou, Y. L. Huang, and W. Chen, Chem. Mater. **34**, 10651 (2022).
[51] C. Hogan, P. Lechifflart, S. Brozzesi, S. Voronovich-Solonevich, A. Melnikov, R. Flammini, S. Sanna, and K. Holtgrewe, Phys. Rev. B **104**, 245421 (2021).
[52] J. Xie, M. Si, D. Yang, Z. Zhang, and D. Xue, J. Appl. Phys. **116**, 073704 (2014).
[53] Y. S. Liu, X. Zhang, X. F. Yang, X. K. Hong, J. F. Feng, M. S. Si, and X. F. Wang, Phys. Chem. Chem. Phys. **17**, 10462 (2015).
[54] J. E. Ortega, G. Vasseur, I. Piquero-Zulaica, S. Matencio, M. A. Valbuena, J. E. Rault, F. Schiller, M. Corso, A. Mugarza, and J. Lobo-Checa, New J. Phys. **20**, 073010 (2018).
[55] A. Jain, S. P. Ong, G. Hautier, W. Chen, W. D. Richards, S. Dacek, S. Cholia, D. Gunter, D. Skinner, G. Ceder *et al.*, APL Mater. **1**, 011002 (2013).